Journal of Biomechanics 45 (2012) 1028–1035

Contents lists available at SciVerse ScienceDirect

Journal of Biomechanics

journal homepage: www.elsevier.com/locate/jbiomech
www.JBiomech.com

Shape optimization of stress concentration-free lattice for self-expandable Nitinol stent-grafts

Ehsan Masoumi Khalil Abad [a], Damiano Pasini [a,*], Renzo Cecere [b]

[a] Mechanical Engineering Department, McGill University, Montreal, Quebec, Canada
[b] McGill University Health Center, McGill University, Montreal, Quebec, Canada

ARTICLE INFO

Article history:
Accepted 1 January 2012

Keywords:
Optimization
Nitinol
Stent-graft
FEM

ABSTRACT

In a mechanical component, stress-concentration is one of the factors contributing to reduce fatigue life. This paper presents a design methodology based on shape optimization to improve the fatigue safety factor and increase the radial stiffness of Nitinol self-expandable stent-grafts. A planar lattice free of stress concentrators is proposed for the synthesis of a stent with smooth cell shapes. Design optimization is systematically applied to minimize the curvature and reduce the bending strain of the elements defining the lattice cells. A novel cell geometry with improved fatigue life and radial supportive force is introduced for Nitinol self-expandable stent-grafts used for treating abdominal aortic aneurism. A parametric study comparing the optimized stent-graft to recent stent designs demonstrates that the former exhibits a superior anchoring performance and a reduction of the risk of fatigue failure.

1. Introduction

Intravascular stents are primarily used to open and scaffold tubular passages or lumens such as blood vessels, biliary ducts and the esophagus (Duerig et al., 1999). They usually consist of an expandable lattice mesh that can deploy and hold endovascular grafts, arterial endoprosthesis and self-expanding heart valve implants. Figs. 1(a-e) shows recent commercial applications of stent devices, which are designed to deploy into the body by minimally invasive percutaneous intervention (Kleinstreuer et al., 2008; Rose et al., 2001; Vergnat et al., 2009; Webb, 2008).

Depending on the stent application, stents should address multiple functional requirements, which are often antagonist. For example, bare metal stents used for opening the occluded arteries should provide a combination of high radial force and axial flexibility in order to keep the artery open, prevent stent migration, conform to the curved blood vessels, and flex during the body movement (Cheng et al., 2006). In endovascular repairs for abdominal aortic aneurisms (*AAAs*), the structure of a stent-graft should provide sufficiently high radial force to prevent graft migration and blood leakage into the aneurysm cavity (Kleinstreuer and Li, 2006; Kleinstreuer et al., 2008).

Since 1990, an ever increasing demand for endovascular stents has led to significant advancements in the field of analysis, modelling and design of stent implants (Chua et al., 2002; Duerig et al., 1999; Martin and Boyle, 2010; Petrini et al., 2004; Migliavacca et al., 2002; Lim et al., 2008; Lally et al., 2005; Timmins et al., 2007; Bedoya et al., 2006; Wang and Masood, 2006). The results of these studies have shown that besides mechanobiological factors, the geometry and typology of a stent are crucial aspects governing the device function. Shape and size, as well as the thickness of a lattice cell, are geometric variables that can be tailored through design optimization to improve alternative performance metrics, such as fatigue life, axial and radial stiffness among others. So far, however, approaches for the synthesis of optimized lattice geometry have received minor attention. For example, Fig. 1(f) shows the structural geometry of a recent stent consisting of a 2D lattice of closed cells (Zhi et al., 2008). At the blending points between the arcs and the linear segments of each cell, the curvature is not smooth. A curvature discontinuity acts as a stress concentrator (Neuber, 1967), which amplifies its detrimental effect for fatigue loading. This loading condition is ordinary in a ten-years life of a stent, which can undergo nearly four hundred millions of cycles due to pulsating blood pressure and body movement.

Stent fatigue, graft migration, and blood leakage into the aneurysm cavity undermine function and performance of stent grafts (Kleinstreuer and Li, 2006). Two strategies were proposed to reduce these risks: i) stiffen the stent in the radial direction to reduce endovascular leakage and device migration; ii) increase fatigue life by reducing the level of the alternating strain generated by a pulsating blood pressure.

The issue of reducing the level of stress concentration, thereby improving fatigue resistance, motivates this paper. We present a design strategy, which is expressed in the form of mathematical rigour and design optimization, to synthesize a planar lattice free

* Correspondence to: Room 372, Macdonald Engineering Building, 817 Sherbrooke street west, Montreal, Quebec, H3A 2K6 Canada. Tel.: +1 514 398 6295; fax: +1 514 398 7365.
E-mail addresses: ehsan.masoumikhalilabad@mail.mcgill.ca (E. Masoumi Khalil Abad), damiano.pasini@mcgill.ca (D. Pasini), renzo.cecere@muhc.mcgill.ca (R. Cecere).

0021-9290/$ - see front matter © 2012 Elsevier Ltd. All rights reserved.
doi:10.1016/j.jbiomech.2012.01.002

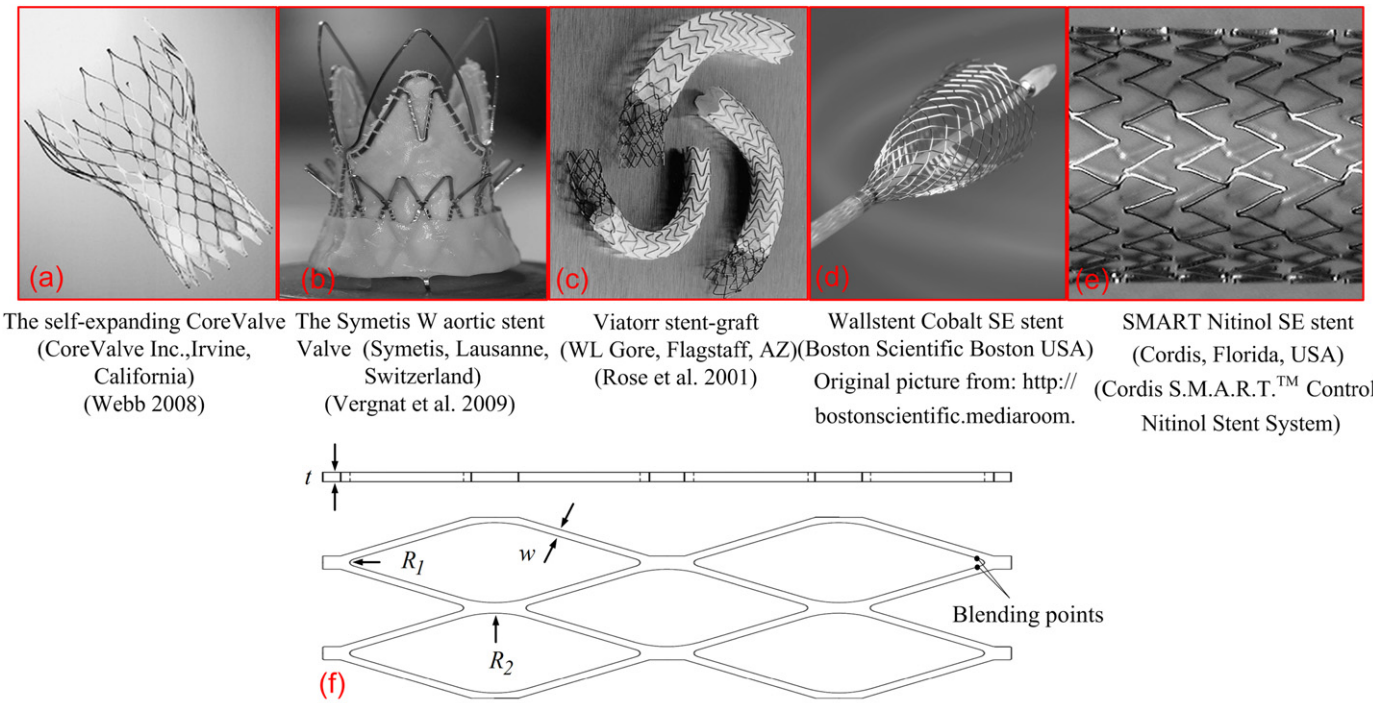

Fig. 1. Commercially available stents developed for prescribed applications.

of stress-concentration for a stent graft. Due to the existence of several stent applications, each entailing the fulfillment of specific requirements, we focus on stent grafts used for treating abdominal aortic aneurism. The results are compared with those obtained by (Kleinstreuer et al., 2008), and discussed through a parametric study to investigate the effect of selected geometric parameters, e.g. tube thickness, strut width, and number of lattice cells, on stent fatigue life and radial supportive force.

2. Shape synthesis of lattice geometry

2.1. Lattice cells with smooth shape elements

In a 10 years expected design life, stents and stent grafts undergo nearly 4×10^8 cycles of alternating forces arising from pulsating blood pressure and body movement (Pelton et al., 2008). Such a loading condition could potentially lead to fatigue failure, especially for stent grafts made of Nitinol, which has a lower resistance to fatigue crack growth in comparison to other metals (Pelton et al., 2008; Stankiewicz et al., 2007; Robertson et al., 2007; McKelvey and Ritchie, 2001).

Stress concentrators perturb locally the stress flow in a component at the location where its geometry changes abruptly. The stress regimes is altered with peaks that has the impact of reducing both static and fatigue resistance (Neuber, 1961a). Neuber first demonstrated the detrimental effect of notches and other stress concentrators on the monotonic and cyclic strength of mechanical components (Pedersen, 2007; Neuber, 1961a; Pilkey, 2007; Williams, 1952; Dunn et al., 1997). He showed that the stress regime locally increases if the radius of curvature of the geometric profile of an element changes discontinuously (Neuber, 1961a). (Neuber, 1961b) showed that under pure shear loading condition the elastic stress concentration is equal to the product of the notch stress concentration factor and the strain concentration factor. Later studies (Topper et al., 1969; Walker, 1970) showed that this relationship is valid also for other static and cyclic stress regimes. It has been shown that by controlling the curvature of a fillet, the stress flow might be smoothed to decrease stress peaks. For instance, (Waldman et al., 2001) showed that under repeated tension and bending the optimized-shape fillet of a shaft shoulder can provide 23% higher fatigue life than a circular-shape fillet.

Fig. 1(f) shows the geometry of a common stent (Zhi et al., 2008). The mesh elements are filleted at the blending points, where their tangent changes continuously. The stent, however, at each blending point exhibits curvature discontinuity which triggers stress concentration and thus accelerates fatigue failure. To remove the occurrence of geometry discontinuity in a stent, we propose here to synthesize the unit cell of a planar lattice with curves that are continuous in their curvature (Teng et al., 2008). Through the formulation of a structural optimization problem explained in the next section, we first impose that each cell members be G^2-continuous at the blending points with adjacent elements and then be *as straight as possible*, i.e. with the smallest possible curvature, to reduce the high bending strains caused by curved cell members.

Fig. 2 shows the unit cell of a stent lattice consisting of G^2-continous curves. The unit cell is repeated in a planar sheet to form the lattice, which is then folded into a cylindrical surface. The stent is described by n_c cells in the circumferential direction and n_l cell rows in the longitudinal direction. The tube thickness and strut width are respectively t and w, the stent length is assumed to be 100 mm and the non-shrunk diameter 30 mm (Kleinstreuer et al., 2008). Next sections describe the procedure to synthesize smooth lattice cell topologies for a Nitinol stent-graft.

2.2. Mathematical formulation of the optimization problem

The problem entails the search of lattice cells with G^2-continuous curves that have minimum root mean square, or *rms,* value of the curvature (Teng et al., 2008). The first stage of the shape synthesis

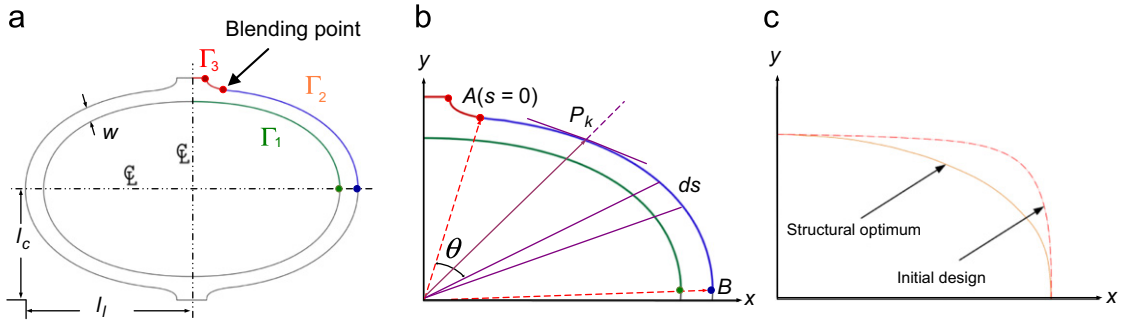

Fig. 2. Schematic view of the proposed G^2-continuous cell geometry: (a) The proposed E cell geometry; (b) Parameterization required for the synthesis of a G^2-continuous cell shape; (c) Inner boundaries of initial design and structurally optimized *E* cell.

involves geometry optimization, in which only the *rms* value of the curvature of the cell elements is minimized. At this step, the material properties of Nitinol are ignored. The second stage entails the structural optimization of the unit cell and requires accounting also for the attributes and stress-strain curve of the material.

The shape synthesis of a cell geometric primitive is stated as follows: under given end conditions, find a boundary-curve Γ that connects two given end points A and B of the cell strut as smoothly as possible and with a G^2-continuous curve. By parametrizing the strut boundary-curve Γ as a function of the arc-length s along the strut, we can formulate the optimization problem as (Teng et al., 2008):

$$J(\Gamma)=\frac{1}{L}\int_A^B \kappa^2 ds \rightarrow \min_{\Gamma(s)} \tag{1}$$

where $\sqrt{J}$ is the *rms* value of the curvature of a cell member boundary-curve, L is the member length, A and B are its end-points, and ds is the arc-length along the member, starting from *0* at point *A*, as shown in Fig. 2(b). The member boundary-curve is subjected to four constraints at each end-point. Two constraints define the end-points coordinates, the other two set the tangent and curvature of the curve at these points.

Eq. (1) can be treated as a problem of mathematical programming by means of non-parametric cubic splines (Spath, 1995). Hence, each boundary curve is discretized by $n+2$ supporting points $\{P_k\}_0^{n+1}$ that are defined by $P_k(\rho_k,\theta_k)$ in a polar coordinate system. As shown in Fig. 2(b), P_k is a generic point of the curve; $P_0=A$ and $P_{n+1}=B$, where $A(\rho_A,\theta_A)$, and $B(\rho_B,\theta_B)$ are two end-points of the boundary-curve of each cell element. Moreover, if we assume that the discrete points are located at constant tangential intervals, the tangential increment will be:

$$\Delta\theta=\frac{\theta_B-\theta_A}{n+1} \tag{2}$$

A cubic spline, $\rho(\theta)$, between two consecutive supporting points P_k and P_{k+1} can be defined as:

$$\rho(\theta)=A_k(\theta-\theta_k)^3+B_k(\theta-\theta_k)^2+C_k(\theta-\theta_k)^2+D_k \tag{3}$$

The radial coordinates, the first and second derivatives of the cubic splines at the kth supporting point, ρ,ρ' and ρ'', respectively, are represented by the following three vectors:

$$\begin{aligned}\rho&=[\rho_0,\rho_1,\ldots\rho_n,\rho_{n+1}]^T\\ \rho'&=[\rho'_0,\rho'_1,\ldots\rho'_n,\rho'_{n+1}]^T\\ \rho''&=[\rho''_0,\rho''_1,\ldots\rho''_n,\rho''_{n+1}]^T\end{aligned} \tag{4}$$

Imposing the G^2-continuity condition results in the following linear relationships between ρ and ρ'' and between ρ and ρ':

$$\boldsymbol{A\rho''}=6\boldsymbol{C\rho}\ \textit{and}\ \boldsymbol{P\rho'}=\boldsymbol{Q\rho} \tag{5}$$

where **A**, **C**, **P**, and **Q** are defined in appendix *A* (Teng et al., 2008). Furthermore, $\rho_0=\rho_A$ and $\rho_{n+1}=\rho_B$ are known from a given parameter vector of the cell. Now, if $\boldsymbol{x}$ is the vector of the design variables, defined as

$$\boldsymbol{x}=[\rho_1,\ldots\rho_n]^T \tag{6}$$

the discretized shape optimization problem can be written as (Teng et al., 2008)

$$z(\boldsymbol{x})=\frac{1}{n}\sum_1^n w_k\kappa_k^2\rightarrow\min_{\boldsymbol{x}} \tag{7}$$

where w_k is the weighting coefficient of point kth defined at each supporting point, and representing the contribution of each point on the curvature of the optimum curve. Furthermore, the curvature at each point P_k is given by:

$$\kappa_k=\frac{\rho_k^2+2(\rho'_k)^2-\rho_k\rho''_k}{(\rho_k^2+(\rho'_k)^2)^{3/2}} \tag{8}$$

Discretizing the objective function (Eq. (7)) and applying the constraints at the end points of the boundary curve, allow solving the problem with mathematical programming. The required number of supporting points depends on the geometric boundary conditions. After performing a sensitivity analysis, 100 supporting points have been selected for the boundary curves. To solve the optimization problem, we used a sequential quadratic programming algorithm employing orthogonal decomposition algorithm. The details of this method can be found in the work of (Teng and Angeles, 2001).

As written previously, the first stage of geometry optimization assumes equal weighting coefficients, i.e. $1/n$, to find a geometrically optimum boundary of the unit cell. This result is then further optimized at a second stage, in which the stress and strain regimes are taken into account. In this case, the expressions of the weighting coefficients, w_k (Eq. (7)) are considered as a function of the strain regime obtained iteratively at each *FEA* iteration. We consider strain, rather than stress as used by (Teng et al., 2008), since the plateau region of the Nitinol stress-strain curve (Fig. 3), which corresponds to the stress induced phase transformation from the austensite to the martensite state, is much more sensitive to strain changes. This has a strong impact on the alternating strain and thus on the fatigue life of Nitinol. The weight coefficients are therefore not uniform along the cell strut boundary-curve and they are defined as:

$$w_k=\frac{\bar{\varepsilon}_k}{\bar{\varepsilon}_T} \tag{9}$$

where $\bar{\varepsilon}_k$ and $\bar{\varepsilon}_T$ are, respectively, the *rms* value of the von Mises strain at the kth supporting point of the profile curve, and the *rms* value of the strain over the whole cell element of the stent and are

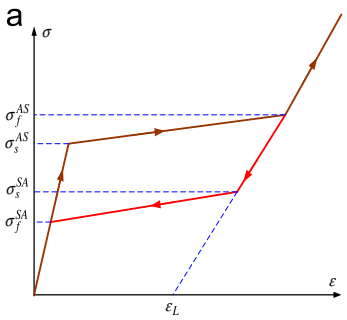

b

Martensit phase Young modulus	47.8GPa
Austenite phase Young modulus	51.7GPa
ν	0.3
σ_s^{AS}	600MPa
σ_f^{AS}	670MPa
σ_s^{SA}	288MPa
σ_f^{SA}	254MPa
ε_L	6.3%

Fig. 3. (a) Schematic view of Nitinol stress-strain curve; (b) Material constants used in the present study (Kleinstreuer et al., 2008).

defined as:

$$\bar{\varepsilon}_T = \sqrt{\frac{1}{m}\sum_{i=1}^{m}\varepsilon_i^2} \tag{10}$$

$$\bar{\varepsilon}_k = \sqrt{\frac{1}{\mu_k}\sum_{i=1}^{\mu_k}\varepsilon_{ki}^2}, \quad \mu_k = \frac{m}{50} \tag{11}$$

where m is the total number of nodes in the FE model, ε_i is the von Mises strain at ith node and ε_{ki} is the von Mises strain of the μ_k nodes (2% of the total nodes of FE model), which are relatively closer to the kth supporting point. The optimization algorithm is set to end when the reduction in the maximum strain value is smaller than 0.1%.

2.2.1. Finite element modeling

Usually, a stent consists of a set of separate rows that are sutured on the graft fabric. Between rows, there is a gap in the axial direction to allow a relative movement of the stent rows and to increase the axial flexibility of the stent. Since in the sealing section, located at the two distal rows of the stent-graft, the stent does not gain its original size and the graft material is not in tension, and since the graft material has negligible stiffness, the effect of the connectivity of the rows in the sealing section can be ignored (Kleinstreuer et al., 2008). Hence in this work, only the stent rows in contact with the aneurism neck are examined due to their importance for stent-graft migration and fatigue life (Kleinstreuer et al., 2008).

The stent geometry is automatically synthesized through an in-house MATLAB subroutine, which is coupled to ANSYS to build, mesh, and solve the *3D* model of the stent. Because of symmetry in both geometry and loading, only ¼ of one cell is modeled. Symmetric boundary conditions are applied at the planes of symmetry. To mesh the stent elements of the lattice cell, a 3D eight-node element type, *SOLID 185*, is selected. The arterial wall is modeled as a cylinder and meshed by a twenty-node element type, *SOLID 95*. A mesh sensitivity test is also performed to ensure the independency of the results from the mesh size.

2.2.2. Material model

Nitinol is a pseudo-elastic material extensively used in bio-medical devices for its bio-compatibility, shape memory property besides outstanding ability to withstand severe deformation. Fig. 3 is a schematic view of the stress-strain curve of Nitinol at a given temperature. To model the super-elasticity characteristics of Nitinol, we use the constitutive model presented by (Auricchio, 1995) with material properties shown in Fig. 3(b).

The structure of the artery wall is assumed to be incompressible with a Young modulus of 1.2 MPa and a Poisson ratio of 0.495, as prescribed by FDA protocols (ASTM, 2007).

2.2.3. Loading conditions

a. Shrinking loading
For delivery purposes, the stent-graft with outer diameter of 30 mm must be first shrunk to fit into the 24 F delivery sheath and then, when deployed, must regain its original shape. We model the shrinking manoeuvre by applying a radial displacement to a rigid movable surface, which is in frictionless contact with the strut outer surface. The graft material is assumed to have a negligible effect on the overall behaviour of the stent in the sealing section; thus the graft is not considered in the model.

b. Sealing loading
The stent should be anchored to the neck artery of the abdominal aortic aneurism (*AAA*) after its release from the deployment system. The anchoring force should be sufficiently high to prevent the stent-graft migration. In this study, the stent deployment is modeled in two steps. First, the stent is shrunk to a diameter close to the artery interior wall by using rigid contact surface. Second, the stent expanded to reach an equilibrium radius in contact with the artery wall by gently removing the contact surface of the rigid body. The diastolic and systolic blood pressures are modeled as constant pressures applied to the inner surface of the artery wall.

3. Results

Fig. 2(c) shows the results of minimizing the curvature of the inner boundary-profile for the *E* lattice cell. Fig. 4 shows the views of the structurally optimized stents.

Fig. 5(a) illustrate the von Mises strain distribution in the shrunk stent. It can be seen that the maximum strain level is below 12%, the allowable threshold strain limit of Nitinol (Kleinstreuer et al., 2008); the stent can thus shrunk without fracture. The distribution of the first principal strain in the deployed stents is shown in Fig. 5(b). Table 1 shows the performance of the proposed design in comparison with the *R* stent (Kleinstreuer et al., 2008). We note that the requirement used for comparison is the area of the *R* stent in contact with the artery; this value is assumed to be equal to the area of the *E* stent. As explained in the discussion, the deployment constraint imposes a maximum on the allowable number of cells in the circumferential direction. For a given surface area requirement, we select the strut width as design variable and we fix as design parameters: 1) the number *of cells in the longitudinal direction* so as the stents have equal share of pressure on the artery wall at each row; 2) *the stent thickness*, as its effect on the blood flow and hemodynamic properties is significant. Table 1 shows that the proposed *E* stent

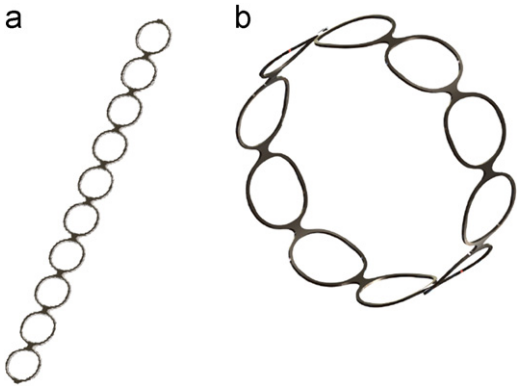

Fig. 4. Structurally optimized stent. (a) A straight row of lattice cells, (b) A row folded into a cylinder.

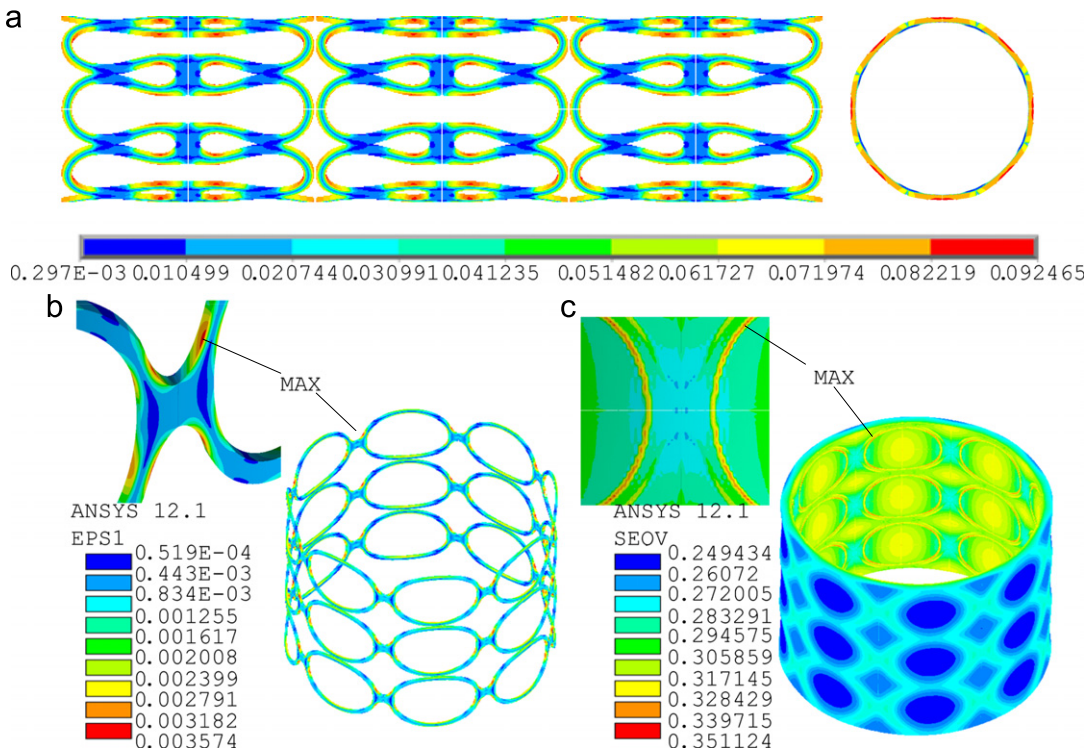

Fig. 5. FEA results for *E* cell geometry. (a) Strain distribution in the shrunk stent; (b) First principal strain in the stent after stent deployment under 100 mm-Hg mean pressure.; (c) Von Mises stress (in MPa) distribution in the artery after stent deployment under 100 mm-Hg mean pressure. The maximum value occurs at the interface between stent and artery wall.

Table 1
Comparison of stent performances. R cell from (Kleinstreuer et al., 2008).

xz	Radial force at 100 mmHg (N)	Fatigue safety factor	Wall stress (MPa)	Maximum shrunk strain (%)
E cell	3.1	3.4	0.351	9.42
R cell	1.7	2.01	0.265	8.86

has 69.1% higher fatigue safety factor[1] and 82.4% larger radial supportive force per unit of stent area. Fig. 5(c) shows the von Mises stress distribution induced in the artery wall after graft deployment. The stress level in the artery wall is below 0.67 MPa, the elastic limit of the artery (Raghavan et al., 1996). However, compared to the *R* stent, the level of von Mises stress induced in the artery wall exhibits a 32.4% increase. Although this stress level might reduce over time, it should be always below the allowable elastic limit of the artery wall after stent insertion.

Fig. 6 illustrates the radial supportive force as a function of the outer diameter for *E* stent in comparison with the *R* stent for a prescribed stent area and tube thickness. For a 2 mm constant radial displacement, the proposed *E* cell design provides 165% increase in the supportive radial force.

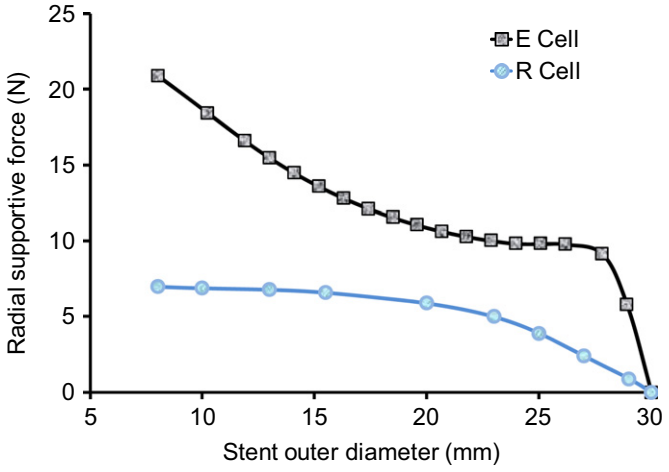

Fig. 6. Radial supportive force versus stent outer diameter of *E*-stents compared to *R* cell stent (Kleinstreuer et al., 2008) for a given area in contact with the artery wall. The design parameters for *E*-stent are $n_c=8$, $n_l=10$, $t=0.28$ mm, $w=0.45$ mm, while those for *R* stent are $n_c=20$, $n_l=10$, $t=0.28$ mm, $w=0.35$ mm (Kleinstreuer et al., 2008).

4. Discussion and concluding remarks

To discuss the effect of the changes in the geometry of the optimized stent geometry, we have performed a parametric study that assesses the role of n_c, n_l, t, and w on the (i) deployed stent supportive radial force under 100 mmHg blood pressure; ii) stent fatigue safety factor; and iii) stent area. Fig. 7 summarizes the results. As can been seen, the application of the proposed methodology enables to find lattice structures with higher fatigue safety factor and an improved radial supportive force. In particular, for a 25% increase of n_c, n_l, t, and w, the radial supportive force increases respectively by 1.4%, 18.55%, 7.39%, and 2.11%. The fatigue safety factor improves by 49.7%, 45.5%, 50.7%, and 41.6%. The stent area also increases of 14.7%, 14.8%, 16.1% and 0%. The above benefits come along with a side-effect, i.e. an increase of the level of von Mises stress induced in the artery wall. This is

[1] Fatigue safety factor $= \frac{\text{Nitinol alternating strain limit}(\varepsilon_{all})}{\text{Alternating strain of stent}(\varepsilon_{alt})}$ where $\varepsilon_{all}=0.4\%$ (Pelton et al., 2004) and $\varepsilon_{alt}=0.5$ (strain at 150 mm Hg−strain at 150 mm Hg).

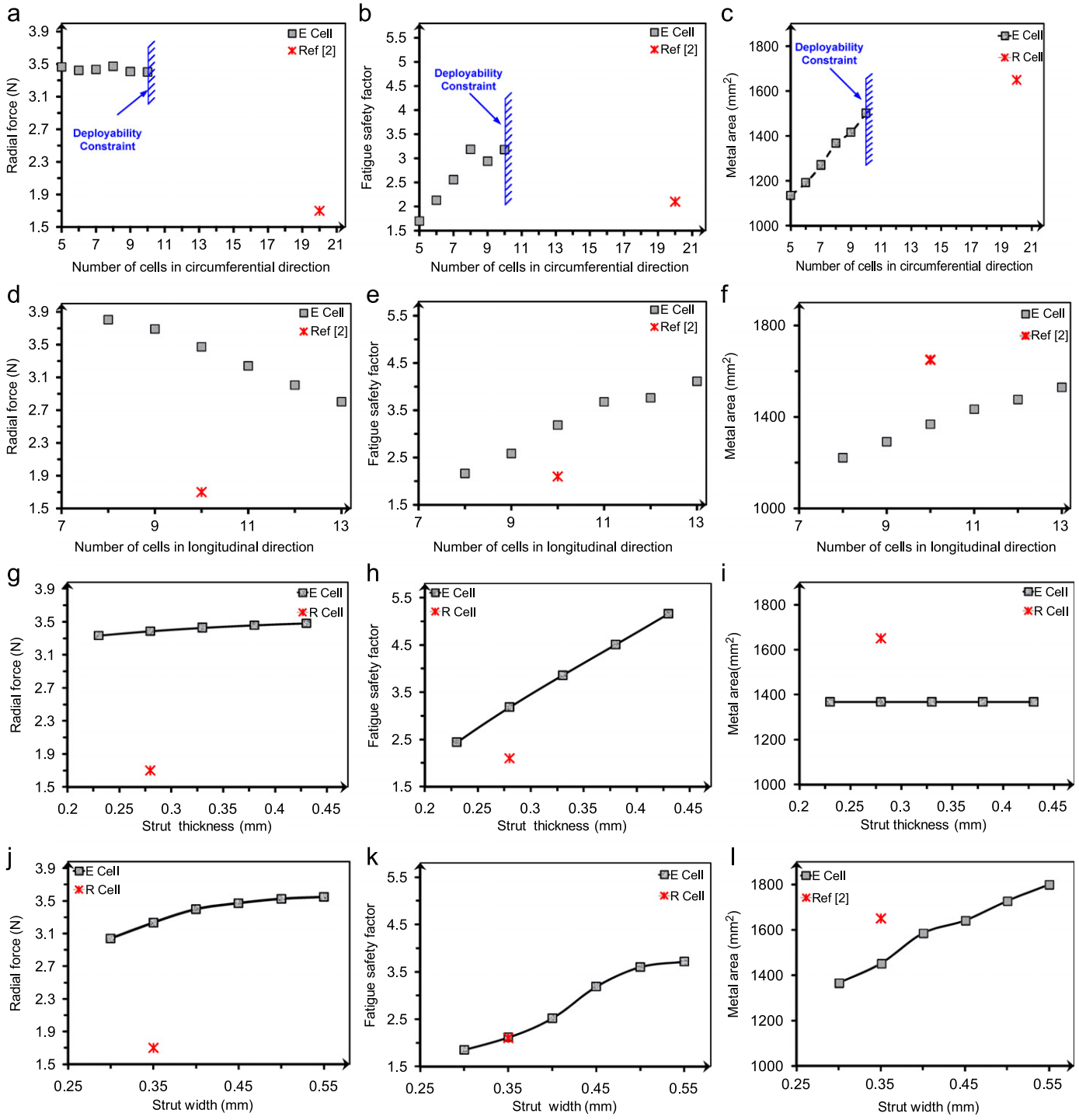

Fig. 7. Plots of number of cells in the circumferential and radial direction, thickness and width of cell elements versus radial force, fatigue safety factor, and metal area in contact with the artery for *E* cell geometry. (a–c) effect of n_c for, n_l=10, t=0.28 mm, w=0.45 mm (d–f) effect of n_l for t=0.28 mm, w=0.45 mm, n_c=8; (g–i) effect of t for, w=0.45 mm, n_l=10, n_c=8; (j–l) effect of w for, t=0.28 mm, n_l=10, n_c=8 for *E* cell geometries. *R* stent is a benchmark stent design (Kleinstreuer et al., 2008); its design parameters are n_c=20, n_l=10, t=0.28 mm, w=0.35 mm.

mainly caused by a higher radial supportive force applied by the sharp edges of the stent struts in contact with the artery wall. However, despite the higher stress level in the artery wall, the contact stress is distributed more uniformly around the artery wall. Furthermore, this stress level can be easily reduced by smoothing the sharp fillet of the strut edges of the stent in contact with the artery.

The results of the parametric study show that to obtain a shrinkable stent an upper limit is required on the number of cells in the circumferential direction. For example, Figs. 7(a–c) show that for a stent with n_l =10, t=0.28 mm, w=0.45 mm, only values of n_c less than 10 enable the stent to can be shrunk without fracture.

The impact of the number of cells in the circumferential direction, n_c, is illustrated in Figs. 7(a–c). Whereas the supportive radial force of the stent is not affected, the stent area shows a rapid linear increase. The stent fatigue safety factor, on the other hand, decreases if n_c reduces. Therefore, higher values of n_c should

be chosen while respecting the deployment constraint (Fig. 7(a)). It is worthy to mention, also, that reducing n_c might increase the stress level in the artery wall.

Figs. 7(d–f) illustrate the influence of the number of cells, n_l, in the longitudinal direction on stent performance. By increasing n_l for a given arterial length, the share of each row in supporting the arterial radial load decreases and reduces the level of radial supportive force (Fig. 7(d)). In addition, the stiffness of the stent increases by shortening the length of each cell row. This outcome improves the stent fatigue safety factor by reducing the level of alternating strain.

Figs. 7(g) and 7(j) show that thickening the strut and width is beneficial for both stent radial stiffness and radial supportive force. Besides these gains, a stiffer stent would be also more resistant to the deformation imposed by a pulsatile pressure, thereby reducing the alternating strain experienced by its members. This is observed in Figs. 7(h) and 7(k), where the fatigue safety factor increases linearly with w and t. On the other hand, Fig. 7(i) shows that the stent area is not affected by any change of the stent thickness as opposed to the trend observed by varying n_c, n_l, w in Figs. 7(c), (f), and (l).

The result of Fig. 7(g), however, should be taken with a caution. A thicker strut will cause a higher contact stress in the artery wall. Furthermore, blood flow in proximity with the artery wall and stent struts will affect the selection of the strut thickness. These issues should be determined through multi-disciplinary analysis and optimization involving both computational fluid dynamics and structural analysis.

The methodology proposed in this paper can be extended to synthesize the geometry of other types of stents, e.g. superficial femoral artery stents, to meet prescribed requirements imposed by a specific application. A fracture mechanics approach, based on the design guidelines for fatigue design of Nitinol devices (Robertson and Ritchie, 2007; Robertson and Ritchie, 2008; Stankiewicz et al., 2007) can also be integrated to further improve the performance of the stent lattice.

Conflict of interest statement

There are no conflicts of interest.

Acknowledgments

This work is funded by the Natural Sciences and Engineering Research Council of Canada (NSERC). The authors thank MD O. Steinmetz, chief of service, Division of Vascular Surgery (McGill University Health center), for providing useful insight into the endovascular techniques used to repair aortic aneurysms.

References

ASTM, I., 2007. Standard test methods for in vitro pulsatile durability testing of vascular stents. ASTM Standard, West Conshohocken, PA. F2477.

Auricchio, F., 1995. Shape Memory Alloys: Applications, Micromechanics, Macromodeling and Numerical Simulations. University of California, Berkely. at.

Bedoya, J., Meyer, C.A., Timmins, L.H., Moreno, M.R., Moore, J.J.E., 2006. Effects of Stent Design Parameters on Normal Artery Wall Mechanics. Journal of Biomechanical Engineering 128 (5), 757–765.

Cheng, C.P., Wilson, N.M., Hallett, R.L., Herfkens, R.J., Taylor, C.A., 2006. In Vivo MR Angiographic Quantification of Axial and Twisting Deformations of the Superficial Femoral Artery Resulting from Maximum Hip and Knee Flexion. Journal of vascular and interventional radiology : JVIR 17 (6), 979–987.

Chua, S.N.D., Mac Donald, B.J., Hashmi, M.S.J., 2002. Finite-element simulation of stent expansion. Journal of Materials Processing Technology 120 (1-3), 335–340.

Duerig, T., Pelton, A., Stöckel, D., 1999. An overview of nitinol medical applications. Materials Science and Engineering A 273-275, 149–160.

Dunn, M.L., Suwito, W., Cunningham, S., 1997. Stress intensities at notch singularities. Engineering Fracture Mechanics 57 (4), 417–430.

Kleinstreuer, C., Li, Z., 2006. Analysis and computer program for rupture-risk prediction of abdominal aortic aneurysms. BioMedical Engineering Online 5 (1), 19.

Kleinstreuer, C., Li, Z., Basciano, C.A., Seelecke, S., Farber, M.A., 2008. Computational mechanics of Nitinol stent grafts. Journal of Biomechanics 41 (11), 2370–2378.

Lally, C., Dolan, F., Prendergast, P.J., 2005. Cardiovascular stent design and vessel stresses: a finite element analysis. Journal of Biomechanics 38 (8), 1574–1581.

Lim, D., Cho, S.-K., Park, W.-P., Kristensson, A., Ko, J.-Y., Al-Hassani, S., Kim, H.-S., 2008. Suggestion of Potential Stent Design Parameters to Reduce Restenosis Risk driven by Foreshortening or Dogboning due to Non-uniform Balloon-Stent Expansion. Annals of Biomedical Engineering 36 (7), 1118–1129.

Martin, D., Boyle, F.J., 2010. Computational structural modelling of coronary stent deployment: a review. Computer Methods in Biomechanics and Biomedical Engineering.

McKelvey, A.L., Ritchie, R.O., 2001. Fatigue-crack Growth Behavior in the Superelastic and Shape-memory Alloy Nitinol. Metallurgical and Materials Transactions A: Physical Metallurgy and Materials Science 32 (Compendex), 731–743.

Migliavacca, F., Petrini, L., Colombo, M., Auricchio, F., Pietrabissa, R., 2002. Mechanical behavior of coronary stents investigated through the finite element method. Journal of Biomechanics 35 (6), 803–811.

Neuber, H., 1961a. Theory of notch stresses: Principles for Exact Calculation of Strength with Reference to Structural Form and Material, 2nd edn. United States Atomic Energy Commission, Washington.

Neuber, H., 1961b. Theory of Stress Concentration for Shear Strained Prismatic Bodies with Arbitrary Nonlinear Stress-Strain Law. Journal of Applied Mechanics, Transactions of the ASME 28, 554.

Neuber, H., 1967. Theory of notch stresses: Principles for Exact Calculation of Strength with Reference to Structural Form and Material, 2nd edn. United States Atomic Energy Commission, Washington.

Pedersen, P., Year. Published Some Benchmarks for Optimized Shapes with Stress Concentration. In Proceeding of the, 2007.

Pelton, A.R., Gong, X.Y., Duerig, T., Year. Published Fatigue testing of diamond-shaped specimens. In Proceeding of the, 2004. Asm Intl, p 199.

Pelton, A.R., Schroeder, V., Mitchell, M.R., Gong, X.-Y., Barney, M., Robertson, S.W., 2008. Fatigue and Durability of Nitinol Stents. Journal of the Mechanical Behavior of Biomedical Materials 1 (2), 153–164.

Petrini, L., Migliavacca, F., Auricchio, F., Dubini, G., 2004. Numerical Investigation of the Intravascular Coronary Stent Flexibility. Journal of Biomechanics 37 (4), 495–501.

Pilkey, W.D., 2007. Frontmatter. In, Peterson's Stress Concentration Factors. John Wiley & Sons, Inc., pp. i-xxxii.

Raghavan, M., Webster, M., Vorp, D., 1996. Ex vivo biomechanical behavior of abdominal aortic aneurysm: Assessment using a new mathematical model. Annals of Biomedical Engineering 24 (5), 573–582.

Robertson, S.W., Mehta, A., Pelton, A.R., Ritchie, R.O., 2007. Evolution of Crack-tip Transformation Zones in Superelastic Nitinol Subjected to in Situ Fatigue: A Fracture Mechanics and Synchrotron X-ray Microdiffraction Analysis. Acta Materialia 55 (18), 6198–6207.

Robertson, S.W., Ritchie, R.O., 2007. In Vitro Fatigue-crack Growth and Fracture Toughness Behavior of Thin-walled Superelastic Nitinol Tube for Endovascular Stents: A Basis for Defining the Effect of Crack-like Defects. Biomaterials 28 (4), 700–709.

Robertson, S.W., Ritchie, R.O., 2008. A fracture-mechanics-based approach to fracture control in biomedical devices manufactured from superelastic Nitinol tube. Journal of Biomedical Materials Research Part B: Applied Biomaterials 84B (1), 26–33.

Rose, J.D.G., Pimpalwar, S., Jackson, R.W., 2001. A new stent-graft for transjugular intrahepatic portosystemic shunts. Br J Radiol 74 (886), 908–912.

Spath, H., 1995. One Dimensional Spline Interpolation Algorithms, Mass. A K Peters, Wellesley.

Stankiewicz, J., Robertson, S., Ritchie, R., 2007. Fatigue-crack growth properties of thin-walled superelastic austenitic Nitinol tube for endovascular stents. Journal of Biomedical Materials Research Part A 81 A 3, 685–691.

Teng, C.P., Angeles, J., 2001. A sequential-quadratic-programming algorithm using orthogonal decomposition with Gerschgorin stabilization. Journal of mechanical design 123 (4), 501–509.

Teng, C.P., Bai, S., Angeles, J., 2008. Shape Synthesis in Mechanical Design. Acta Polytechnica 47 (6), 56–62.

Timmins, L., Moreno, M., Meyer, C., Criscione, J., Rachev, A., Moore, J., 2007. Stented artery biomechanics and device design optimization. Medical and Biological Engineering and Computing 45 (5), 505–513.

Topper, T., Wetzel, R., Morrow, J.D., 1969. Neubers Rule Applied to Fatigue of Notched Specimens. J MATER 4 (1), 200–209.

Vergnat, M., Henaine, R., Kalejs, M., Bommeli, S., Ferrari, E., Obadia, J.-F., Von Segesser, L.K., 2009. A new self-expanding aortic stent valve with annular fixation: in vitro haemodynamic assessment. Eur J Cardiothorac Surg 35 (6), 970–976.

Waldman, W., Heller, M., Chen, G., 2001. Optimal free-form shapes for shoulder fillets in flat plates under tension and bending. International Journal of Fatigue 23 (6), 509–523.

Wang, X., Masood, S., 2006. Investigation of expansion characteristics of coronary slot stents using finite flement analysis. In: Wang, K., Kovacs, G., Wozny, M., Fang, M (Eds.), Knowledge Enterprise: Intelligent Strategies in Product Design, Manufacturing, and Management, vol 207. IFIP International Federation for Information Processing. Springer, Boston, pp. 735–742.

Webb, J.G., 2008. Percutaneous Aortic Valve Replacement Will Become a Common Treatment for Aortic Valve Disease. Journal of the American College of Cardiology: Cardiovascular Interventions 1 (2), 122–126.

Williams, M., 1952. Stress singularities resulting from various boundary conditions in angular corners of plates in extension. J appl Mech 19 (4), 526–528.

Zhi, Y., Wang, X., Gao, Z., Liu, Y., Yue, Z., 2008. Mechanical property analysis of Nitinol defective stent under uniaxial loading/unloading. Materialwissenschaft und Werkstofftechnik 39 (7), 479–485.